Int. J. Solids Structures Vol. 29, No. 9, pp. 1105–1116, 1992
Printed in Great Britain.

0020-7683/92 $5.00 + .00
Pergamon Press plc

THE ROLE OF MATERIAL ORTHOTROPY IN FRACTURE SPECIMENS FOR COMPOSITES

G. BAO
Department of Mechanical Engineering, The Johns Hopkins University, Baltimore, MD 21218, U.S.A.

and

S. HO and Z. SUO
Department of Mechanical Engineering, University of California, Santa Barbara, CA 93106, U.S.A.

and

B. FAN
Materials Department, University of California, Santa Barbara, CA 93106, U.S.A.

(*Received* 2 *March* 1991; *in revised form* 17 *August* 1991)

Abstract—Guided by the orthotropy rescaling technique and other available analytic results, a systematic analysis is conducted for commonly used fracture specimens to investigate the role of material orthotropy in fracture behavior of unidirectional composites. Included are notched bars, delamination beams and hybrid sandwiches, of many varieties. All numerical calibrations are presented with fitting formulae in the relevant parameter regimes. The effect of material orthotropy on fracture behavior of unidirectional composites is thus quantified, which significantly reduces the complexities involved in both experimental investigation and theoretical modelling. A summary of the orthotropy rescaling concepts, with some extensions, is also included.

1. INTRODUCTION

This paper is part of our effort to study the fracture behavior of composite laminates. Several mechanics issues in delamination testing have been studied in recent works. First, laminates are usually anisotropic and heterogeneous, as exemplified by a laminated polymer composite. Delamination specimen calibration is complicated by many elastic constants. The Irwin–Kies compliance calibration is frequently used as a substitute, but the calibration obtained in this way should only be valid for the material being tested, and moreover, mode mixity cannot be determined. An orthotropy rescaling technique has been developed which, as demonstrated by Suo *et al.* (1990), can reduce plane elastic problems for orthotropic materials to equivalent ones for materials with cubic symmetry. The technique has been used to gain insight into the interplay between anisotropy and finite geometry, and study technical problems such as stress concentration related cracking, effective contraction of orthotropic material specimens, mixed mode delamination and crack deflection.

A second issue is that delamination resistance depends strongly on mode mixity, the relative proportion of the opening and sliding. The concepts of mode mixity and toughness surface, as rationalized by Rice (1988) for interfaces in isotropic solids, have been extended to solids of arbitrary anisotropy (Suo, 1992; Wang *et al.*, 1990). It is essential to develop mixed mode specimens in order to have a complete characterization of delamination.

A third issue is the so-called large-scale bridging. Delamination is resisted by intact fibers that cross over crack planes, or by damage in the matrix in the form of voids and micro-cracks. The length of the damage zone is typically several times the beam thickness. Consequently, delamination resistance is no longer a material property independent of specimen geometry and size. The implications have been studied by Bao *et al.* (1990), Suo *et al.* (1992) and Spearing and Evans (1991).

Calibration of fracture specimens plays an important role in both the measuring and modelling of composite fracture and fatigue resistance. However, the existing numerical calibrations are rather complex and sometimes erroneous. Guided by the orthotropy rescaling and other analytical results, we present here a catalog of commonly used fracture

specimens for unidirectional composites. An outline of the orthotropy rescaling method is given in the next section, but readers only interested in specimen calibrations may skip this. Notched bars, delamination beams and hybrid sandwiches are described in the subsequent sections. The scope may be appreciated by looking ahead at the figures in the paper. All numerical calibrations are presented with fitting formulae in the relevant parameter regimes. The effect of orthotropy on the fracture behavior of unidirectional composites is thus quantified, which significantly reduces the complexities involved in both experimental investigation and theoretical modelling, as exemplified by the recent study of fatigue crack growth in a fiber-reinforced metal matrix composite (Bao and McMeeking, 1991).

2. ORTHOTROPY RESCALING

Consider an orthotropic solid in a plane stress state. Plane strain deformation is treated in the Appendix. The coordinates x and y coincide with the principal axes 1 and 2 of the orthotropic material. Two dimensionless parameters, λ and ρ, are defined in terms of the engineering elastic constants (Suo, 1990a, b):

$$\lambda = \frac{E_2}{E_1}, \quad \rho = \frac{(E_1E_2)^{1/2}}{2G_{12}} - (\nu_{12}\nu_{21})^{1/2}. \tag{1}$$

They characterize the in-plane orthotropy: $\lambda = \rho = 1$ for isotropic materials and, $\lambda = 1$ for solids with cubic symmetry. Typical values of λ and ρ are in the range $0.05 < \lambda < 20$ and $0 < \rho < 5$.

Let $U(x, y)$ be the Airy function so that stresses at equilibrium are derived from

$$\sigma_x = \frac{\partial^2 U}{\partial y^2}, \quad \sigma_y = \frac{\partial^2 U}{\partial x^2}, \quad \tau_{xy} = -\frac{\partial^2 U}{\partial x \partial y}. \tag{2}$$

The governing equation is (Lekhnitskii, 1981):

$$\frac{\partial^4 U}{\partial x^4} + 2\lambda^{1/2}\rho \frac{\partial^4 U}{\partial x^2 \partial y^2} + \lambda \frac{\partial^4 U}{\partial y^4} = 0. \tag{3}$$

An inspection reveals that a rescaling of the x-axis:

$$\xi = \lambda^{1/4} x, \tag{4}$$

reduces eqn (3) to

$$\frac{\partial^4 U}{\partial \xi^4} + 2\rho \frac{\partial^4 U}{\partial \xi^2 \partial y^2} + \frac{\partial^4 U}{\partial y^4} = 0. \tag{5}$$

The equation depends on ρ only. The boundary conditions for $U(\xi, y)$ are now changed to

$$\sigma_x = \frac{\partial^2 U}{\partial y^2}, \quad \lambda^{-1/2}\sigma_y = \frac{\partial^2 U}{\partial \xi^2}, \quad \lambda^{-1/4}\tau_{xy} = -\frac{\partial^2 U}{\partial \xi \partial y}. \tag{6}$$

The resultant forces on an arc are

$$T_x = \partial U/\partial y, \quad \lambda^{-1/4} T_y = -\partial U/\partial \xi. \tag{7}$$

With λ-dependence extracted explicitly, the boundary value problem, defined by eqns (5) and (6) on the ξ–y-plane, now has only one material parameter, ρ. Several applications of this idea can be found in Suo *et al.* (1990).

Displacements can be determined by using an auxiliary function $\chi(\xi, y)$, defined by

$$\frac{\partial^2 \chi}{\partial \xi \partial y} = \frac{\partial^2 U}{\partial \xi^2} + \frac{\partial^2 U}{\partial y^2}. \tag{8}$$

Strain compatibility requires that

$$2(1-\rho)\frac{\partial^2 U}{\partial \xi \partial y} = \frac{\partial^2 \chi}{\partial \xi^2} + \frac{\partial^2 \chi}{\partial y^2}. \tag{9}$$

One may confirm that eqn (5) can be derived from eqns (8) and (9) by eliminating χ.

In terms of U and χ, displacements are represented by

$$E_1 u_x = \lambda^{-1/4}[\partial \chi/\partial y - (1+\lambda^{1/2}\nu_{12})\,\partial U/\partial \xi] \tag{10a}$$

$$E_2 u_y = \lambda^{1/2}[\partial \chi/\partial \xi - (1+\nu_{21})\,\partial U/\partial y]. \tag{10b}$$

In particular, the displacement jumps across a plane, with traction continuity maintained, are

$$(E_1 E_2)^{1/2}\lambda^{-1/4}\delta_x = (\partial \chi/\partial y)^+ - (\partial \chi/\partial y)^- \tag{11a}$$

$$(E_1 E_2)^{1/2}\delta_y = (\partial \chi/\partial \xi)^+ - (\partial \chi/\partial \xi)^-. \tag{11b}$$

These equations are valid for cracks and dislocations.

Consider a crack running in the x-direction, which coincides with the principal material axis 1. The stress intensity factors are defined such that the stresses at a distance r ahead of the crack tip are given asymptotically by

$$\sigma_y = \frac{K_I}{\sqrt{2\pi r}}, \quad \tau_{xy} = \frac{K_{II}}{\sqrt{2\pi r}}. \tag{12}$$

The crack opening and sliding displacements at a distance r behind the crack tip are

$$[\delta_y, \delta_x] = 8\left(\frac{1+\rho}{2E_1 E_2}\right)^{1/2}\sqrt{\frac{r}{2\pi}}\,[\lambda^{-1/4}K_I, \lambda^{+1/4}K_{II}]. \tag{13}$$

The energy release rates are related to the stress intensity factors by

$$[G_I, G_{II}] = \left(\frac{1+\rho}{2E_1 E_2}\right)^{1/2}[\lambda^{-1/4}K_I^2, \lambda^{+1/4}K_{II}^2] \tag{14}$$

and the total energy release rate is

$$G = G_I + G_{II}. \tag{15}$$

These crack tip results were derived by Sih *et al.* (1965).

From eqns (6) and (12), the stress intensity factors can be expressed as

$$\lambda^{-3/8}K_I \sim (2\pi\xi)^{1/2}\frac{\partial^2 U}{\partial \xi^2}, \quad \lambda^{-1/8}K_{II} \sim -(2\pi\xi)^{1/2}\frac{\partial^2 U}{\partial \xi\,\partial y}. \tag{16}$$

These combinations are essential in using the orthotropy rescaling.

$$K_I = \sigma\sqrt{\pi a}\, Y(\rho)F(a/b),\quad Y(\rho) = 1+0.1(\rho-1)-0.016(\rho-1)^2+0.002(\rho-1)^3$$

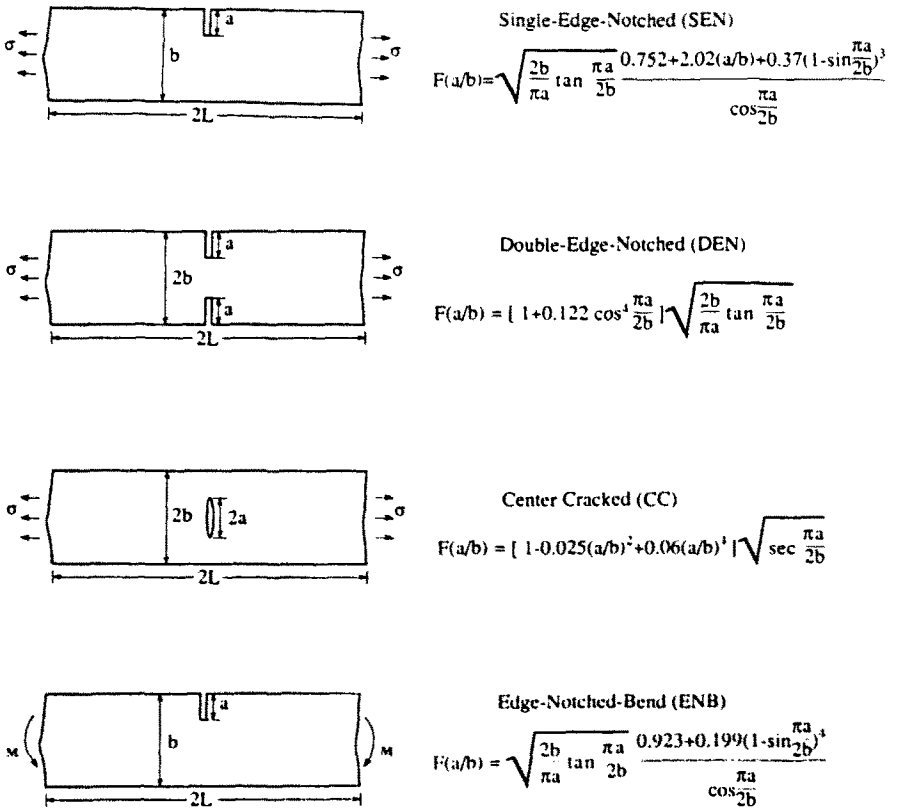

Fig. 1. A family of notched bars. Stress intensity factors are given with the correction factor $Y(\rho)$ due to material orthotropy.

3. NOTCHED BARS

Four notched bars are considered, as shown in Fig. 1. A survey of the relevant literature may be found in Kageyama (1989).

Dimensionality, linearity and orthotropy rescaling dictate that the stress intensity factors take the form:

$$K_I = \sigma\sqrt{\pi a}F(a/b, \lambda^{1/4}L/b, \rho). \tag{17}$$

Here σ is the applied stress for SEN, DEN and CC specimens and

$$\sigma = 6M/b^2 \tag{18}$$

for ENB specimen loaded by the moment M.

Note that in eqn (17), the material parameter λ and the geometric parameter L/b are combined in the way required by orthotropy rescaling. Finite element analysis is used to determine the dimensionless function F. The calculation shows that the effect of $\lambda^{1/4}L/b$ is negligible when $\lambda^{1/4}L/b \geq 2.0$; see Fig. 2. Consequently, this composite parameter is eliminated from the calibration.

Figure 3 reveals the effect of ρ on the stress intensity factors of the SEN specimen. An inspection of the curves suggests an approximate factorization:

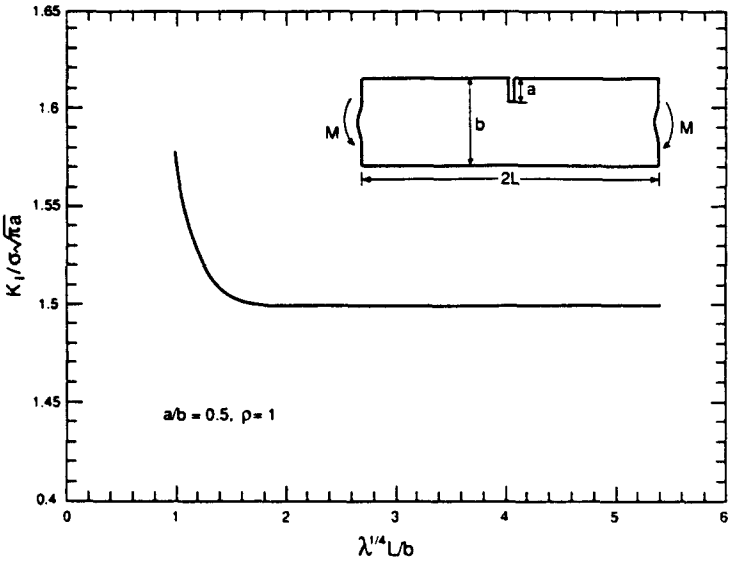

Fig. 2. The stress intensity factor of the notched specimen essentially attains the steady-state when $\lambda^{1/4}L/b = 2$. Values of $a/b = 0.5$, $\rho = 1$ are chosen for the plot, but the same is true for other values of a/b and ρ.

$$K_I = \sigma\sqrt{\pi a}\,Y(\rho)F(a/b). \tag{19}$$

The same is true for DEN, CC and ENB specimens. The geometry dependence, $F(a/b)$, is the same as the corresponding function for an isotropic material (Tada *et al.*, 1985). Our calculations show that, for all four specimens, the factor $Y(\rho)$ can be fitted by a single function:

$$Y(\rho) = 1 + 0.1(\rho - 1) - 0.016(\rho - 1)^2 + 0.002(\rho - 1)^3 \tag{20}$$

with a satisfactory accuracy (error $\leqslant 2\%$ for SEN and ENB; error $\leqslant 5\%$ for DEN and CC).

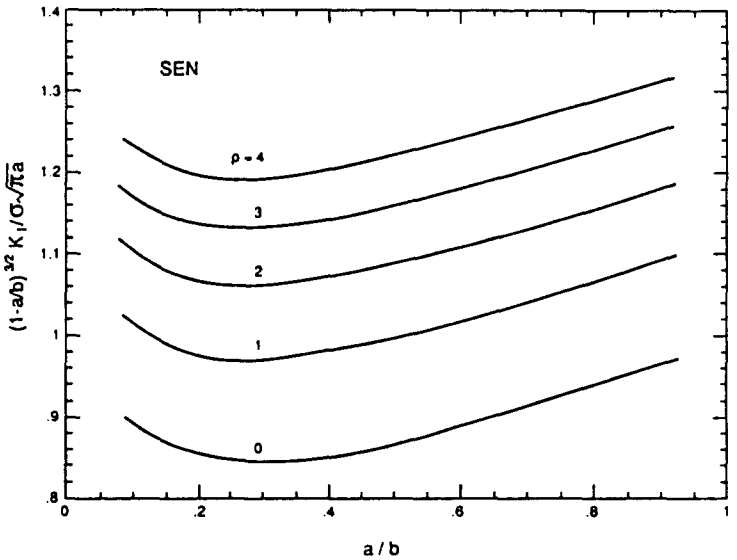

Fig. 3. ρ-dependence of stress intensity factors of single edge notched specimen. It is found that for notched specimens, this ρ-dependence is insensitive to crack length change.

In summary, for materials with $0 \leqslant \rho \leqslant 4$ and any value of λ, the stress intensity factors of the notched bars may be obtained by first taking the corresponding $F(a/b)$ for an isotropic material (reproduced in Fig. 1), and then multiplying by $Y(\rho)$ of (20).

4. MODE I AND MODE II DELAMINATION BEAMS

Depicted in Fig. 4 are the delamination beams most widely used in the composite community. The double-cantilever-beam (DCB) is mode I, and the end-notched-flexure (ENF) and end-loaded-split (ELS) are mode II. Surveys of the relevant literature can be found in Davies and Benzeggagh (1989) and Carlsson and Gillespie (1989).

It has been shown in Suo *et al.* (1990) that the mode I energy release rate for the DCB takes the form:

$$G_{\mathrm{I}} = \frac{12(Pa)^2}{E_1 h^3}[1 + Y_{\mathrm{I}}(\rho)\lambda^{-1.4}h/a]^2, \tag{21}$$

where P is the applied load per unit width of the beam. The first term in the bracket reproduces the result of elementary beam theory, which is an exact elasticity asymptote as $a/h \to \infty$. The second term is the first order correction due to a finite a/h. The factor Y_{I} depends on ρ only. The formula that best fits finite element results is

$$Y_{\mathrm{I}}(\rho) = 0.677 + 0.146(\rho - 1) - 0.0178(\rho - 1)^2 + 0.00242(\rho - 1)^3. \tag{22}$$

Within the practical range $\lambda^{1.4}a/h \geqslant 2$ and $0 \leqslant \rho \leqslant 4$, the error is less than 1%.

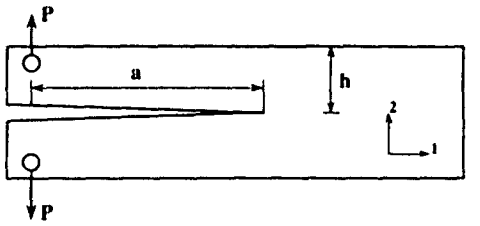

(a) Double-Cantilever-Beam (DCB)

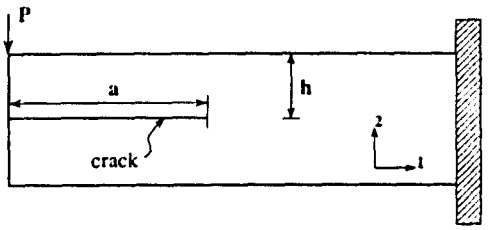

(b) End-Loaded-Split (ELS)

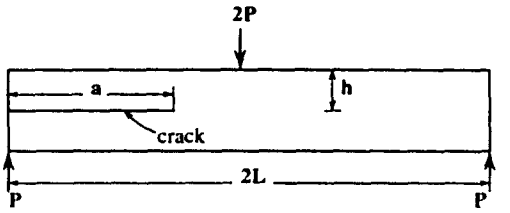

(c) End-Notched-Flexure (ENF)

Fig. 4. Mode I and Mode II delamination beams. P is the load per unit width of the specimen.

For ELS specimen, a similar procedure leads to

$$G_{II} = \frac{9(Pa)^2}{E_1 h^3}[1 + Y_{II}(\rho)\lambda^{-1.4}h/a]^2 \tag{23}$$

where

$$Y_{II}(\rho) = 0.206 + 0.0761(\rho - 1) - 0.00978(\rho - 1)^2 + 0.00112(\rho - 1)^3. \tag{24}$$

The error is less than 1% for $\lambda^{1.4}a/h \geqslant 2$ and $0 \leqslant \rho \leqslant 4$.

An independent finite element calculation (He and Evans, 1991) shows that, for ENF specimen with sufficiently large L/h, the mode II energy release rate has the same calibration as given by (23) and (24), as might be expected.

5. MIXED MODE DELAMINATION BEAMS

Figure 5 illustrates two designs of mixed mode delamination beams. Without loss of generality, attention will be restricted to $H \geqslant h$. Since $G = G_I + G_{II}$, only G and G_I will be presented.

5.1. *Mixed mode double-cantilever-beam*

Guided by elementary beam theory solutions and orthotropy rescaling, we assume that the total energy release rate has the following form:

$$G = \frac{6(Pa)^2}{E_1 h^3}(1 + \eta^3)[1 + Y_I(\rho)B(\eta)\lambda^{-1.4}h/a]^2 \tag{25}$$

where $\eta = h/H$. The factor ahead of the [·] is determined from the simple beam theory

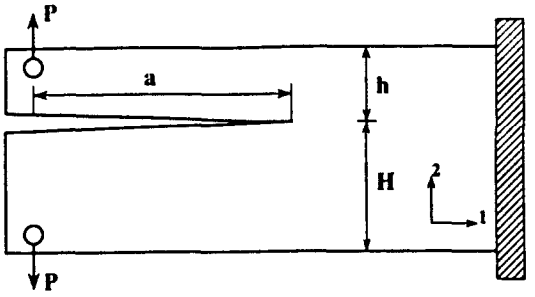

(a) Mixed Mode Double-Cantilever-Beam

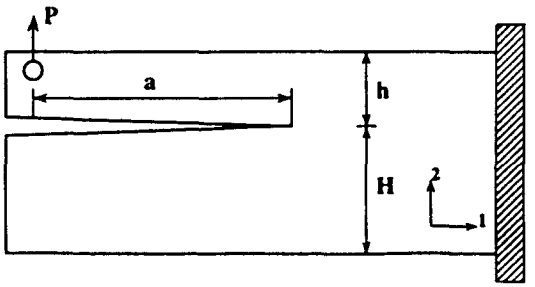

(b) Mixed Mode End-Loaded-Split

Fig. 5. Mixed mode delamination beams.

solution which is the exact asymptote as $h/a \to 0$. Numerical calculations show that the function $Y_1(\rho)$ can be taken to be identical to eqn (22), and the function $B(\eta)$ can be approximated as

$$B(\eta) = 1.120 - 0.695(\eta - 0.585)^2. \tag{26}$$

Within the practical range $\lambda^{1/4}a/h \geqslant 2$, $0.1 \leqslant \eta \leqslant 1$ and $0 \leqslant \rho \leqslant 4$, the error is within 2%.

Our calculations indicate that some elementary rules for partitioning total G into G_I and G_{II} lead to erroneous results. Thus, rigorous finite element results will be used as the basis. The steady-state solution for $a/h \to \infty$ given in Suo (1990) suggests the following form for the mode I energy release rate:

$$G_1 = \frac{6(Pa)^2}{E_1 h^3}(1+\eta^3)\sin^2\phi[1 + Y_1(\rho)B_1(\eta)\lambda^{-1/4}h/a]^2, \tag{27}$$

where Y_1 is given by (22), and

$$B_1(\eta) = 1 + 0.546(1-\eta), \tag{28}$$

and

$$\phi(\eta) = (0.574 + 0.033\eta + 0.805\eta^2 - 0.413\eta^3)\frac{\pi}{2}. \tag{29}$$

The error in eqn (27) is within 2% for $\lambda^{1/4}a/h \geqslant 2$, $0.2 \leqslant \eta \leqslant 1$ and $0 \leqslant \rho \leqslant 4$.

5.2. *Mixed mode end-loaded-split*

It is apparent that the energy release rate for mixed mode ELS with $H = h$ can be obtained by adding eqns (21) and (23). For $H \neq h$, the total energy release rate is

$$G = \frac{6(Pa)^2}{E_1 h^3}[1 - (1 + 1/\eta)^{-3}]\{1 + Y(\rho)(1 + F(\rho)(1-\eta))\lambda^{-1/4}h/a\}^2 \tag{30}$$

where the factor ahead of the $\{\cdot\}$ is determined from the simple beam theory solution which is the exact asymptote as $h/a \to 0$. The factor $Y(\rho)$ in eqn (30) is given by

$$Y(\rho) = 0.484 + 0.122(\rho - 1) - 0.016(\rho - 1)^2 + 0.002(\rho - 1)^3. \tag{31}$$

Fitting numerical results yields:

$$F(\rho) = 0.468\exp(-0.181\sqrt{\rho}). \tag{32}$$

Similar to the mixed mode DCB, the mode I energy release rate for mixed mode ELS is fitted by

$$G_1 = A(\eta)\frac{(Pa)^2}{E_1 h^3}[1 + Y_1(\rho)(1 + F_1(\rho)(1-\eta))\lambda^{-1/4}h/a]^2. \tag{33}$$

The function $A(\eta)$ is given in Suo (1990):

$$A(\eta) = 3.734 - 0.223\eta - 0.867\eta^2 + 0.356\eta^3, \tag{34}$$

while

$$F_1(\rho) = 0.5185 - 0.0244\rho \tag{35}$$

is based on the finite element calculation. Within a 2% error, eqns (30) and (33) are valid for $\lambda^{1/4}a/h \geqslant 2$, $0.2 \leqslant \eta \leqslant 1$ and $0 \leqslant \rho \leqslant 4$.

5.3. *Mode mixity*

The mode mixities of the two specimens in Fig. 5 are usually assumed to remain constant as the cracks grow. This is incorrect if a/h is not very large. Plotted in Fig. 6a, b

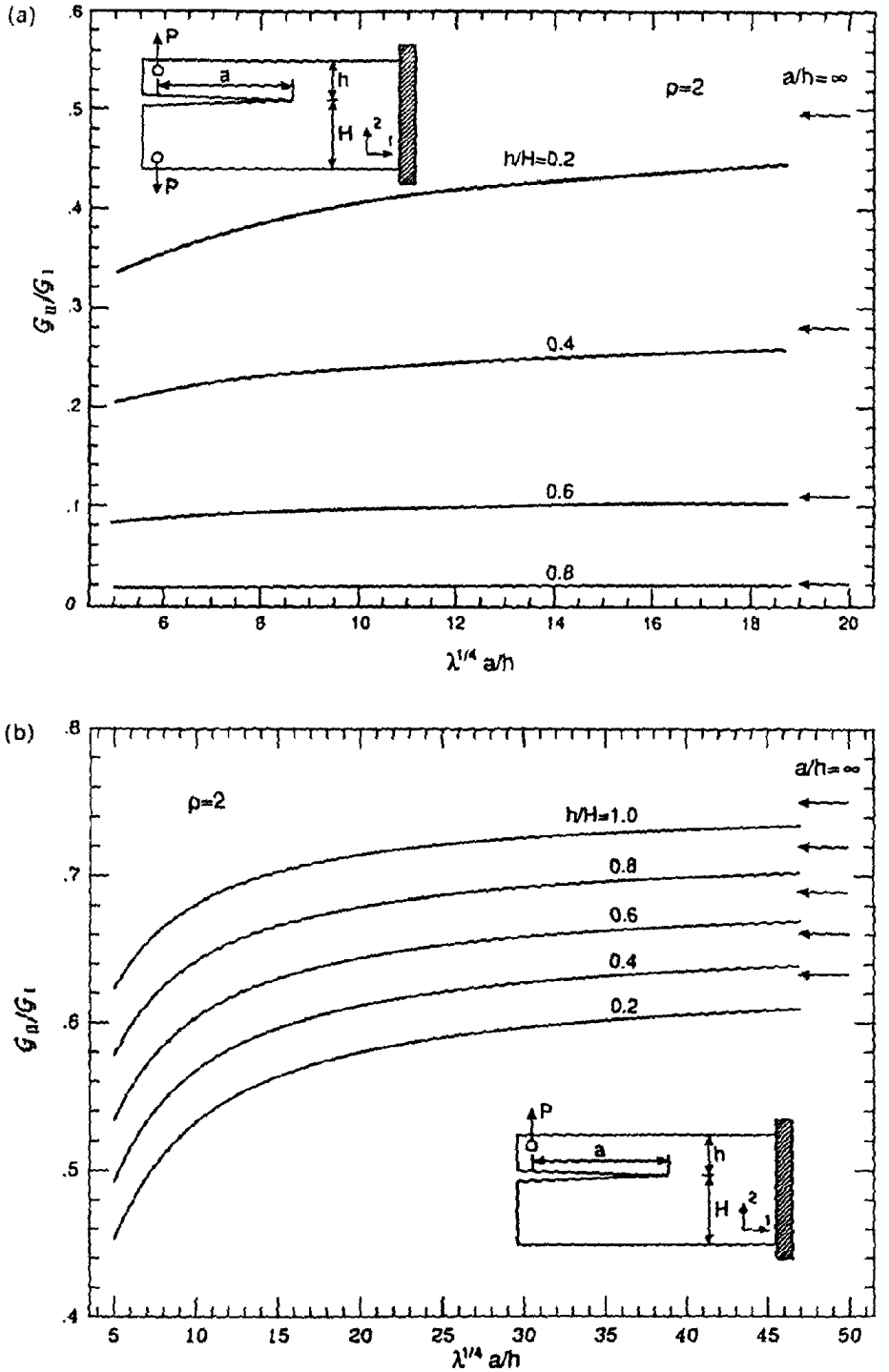

Fig. 6. Mode mixity of mixed mode delamination beams for $\rho = 2$. (a) Mixed mode DCB; (b) Mixed mode ELS. Mode mixity changes with h/H and $\lambda^{1/4}a/h$.

are mode mixities of mixed mode DCB and ELS, respectively. Our calculation indicates that the dependence of mode mixity on material parameter ρ is weak, so only the case $\rho = 2$ is presented.

Observe, first, that the thickness ratio, h/H, has a strong effect on the mode mixity, as might be expected. The mode mixity, specified by the ratio G_{II}/G_I, may vary from zero to 0.6 for the mixed mode DCB and from zero to 0.75 for the mixed mode ELS. Such specimens are therefore suitable for studying mixed mode crack extension in laminates.

Secondly, the mode mixity changes with the effective crack length, $\lambda^{1/4}a/h$. The fixed mode mixities obtained by elementary beam theory solution are asymptotes as $a/h \to \infty$. However, for the mixed mode DCB, the relative changes of mode mixity are less than 10% for $10 \leqslant \lambda^{1/4}a/h \leqslant 20$. For the mixed mode ELS, much larger $\lambda^{1/4}a/h$ is needed to attain the asymptotes.

6. HYBRID SANDWICHES

Hybrid laminates with alternate sheets of ceramics, metals, polymers or composites have been candidates for advanced applications. For such systems, cracking in brittle layers is isolated by the adjacent tough layers, so that the damaged laminates still support the load. Hybrid laminates can also provide additional stiffness for certain experimental needs. For example, in an experimental study of the effect of cross-over fibers on delamination resistance (Spearing and Evans, 1991), the ceramic matrix composite being tested is sandwiched between two alumina layers, in order to provide a higher constraint to obtain a longer bridging zone.

Depicted in Fig. 7 is a hybrid sandwich with a core between two identical skins. The axial force P is applied within the neutral plane of the beam. Each material may be orthotropic with a principal material axis aligned in the beam direction. Young's moduli in the direction of the beam axis for the skins and core are denoted by E^s and E^c, respectively.

We will consider a class of steady-state, mixed mode, hybrid delamination sandwiches, as illustrated in Fig. 8. The energy release rates are independent of crack length, since only axial force and pure moments are applied. Only mode I and mode II loadings are shown in Fig. 8. Friction in mode II specimens (Fig. 8b, d) is neglected; the effect should be independently calibrated. Mixed mode loading can be obtained by superposition. For example, the UCSB four-point-flexure is a superposition of Fig. 8a, b.

The relative stiffness is controlled by two ratios

$$\Sigma = E^s/E^c, \quad \zeta = h/b. \tag{36}$$

The position of the neutral axis is given by

$$\Delta = \frac{\zeta^2 + 2\Sigma\zeta + \Sigma}{2(\zeta + \Sigma)}. \tag{37}$$

The strain field at the three edges far away from the crack tip can be obtained from the elementary beam theory. For example, the axial strain in one of the arms is given by

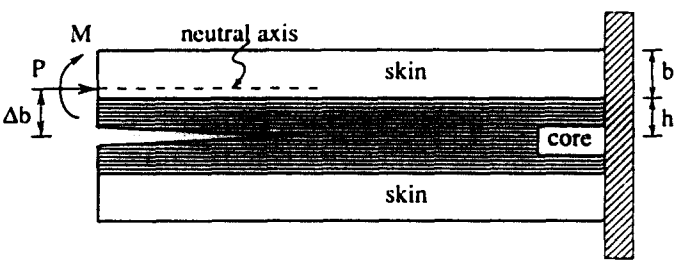

Fig. 7. A hybrid sandwich specimen. The axial force is applied within the neutral plane, which is located at Δb from the crack.

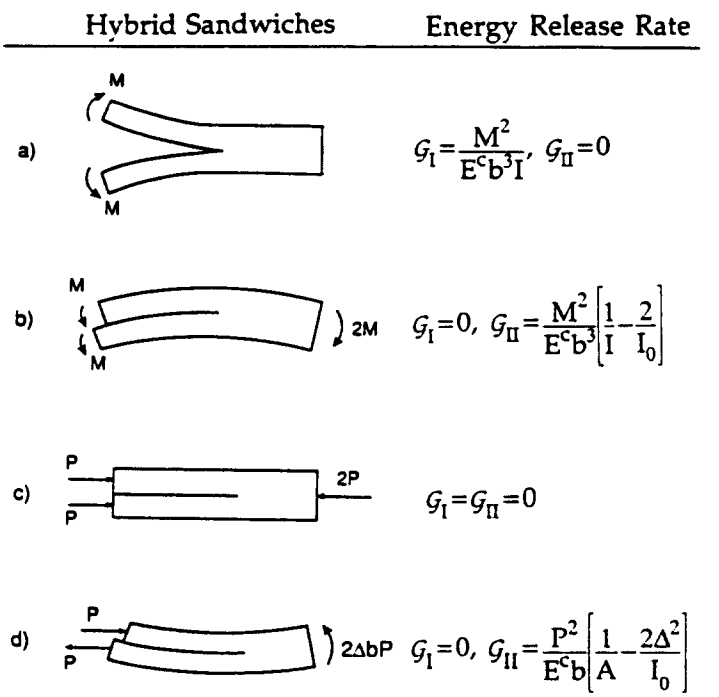

Fig. 8. Energy release rate of hybrid sandwiches. Mixed mode hybrid sandwiches can be obtained by superposition.

$$\varepsilon_x = -\frac{1}{E^c}\left[\frac{P}{Ab}+\frac{My}{Ib^3}\right]. \tag{38}$$

Here y is measured from the neutral axis, P and M are force and moment, A and I are dimensionless cross-section and moment-of-inertia, given by

$$A=\zeta+\Sigma \tag{39a}$$

$$I=\Sigma[(\Delta-\zeta)^2-(\Delta-\zeta)+1/3]+\Delta\zeta(\Delta-\zeta)+\zeta^3/3. \tag{39b}$$

An expression similar to (38) holds for the beam ahead of the crack, with

$$A_0=2(\zeta+\Sigma),\quad I_0=\tfrac{1}{3}[(1-\Sigma)\zeta^3+\Sigma(1+\zeta)^3]. \tag{40}$$

The energy release rate is the difference in the strain energy per unit length stored far behind and far ahead of the crack tip. The results are given in Fig. 8. The mixed mode energy release rate can be obtained by superposition.

7. CONCLUDING REMARKS

The calibration of fracture specimens for unidirectional composites is complicated by many elastic constants. At least two non-dimensional material parameters are involved in the numerical analyses of fracture specimens reported to date. In contrast, by using a spatial rescaling technique, only the effect of $\rho=(E_1E_2)^{1/2}/2G_{12}-(\nu_{12}\nu_{21})^{1/2}$ needs to be calibrated numerically, the dependence of another parameter, $\lambda=E_2/E_1$, is known analytically. In particular, for SEN, DEN, CC and ENB specimens, a single correction factor $Y(\rho)$ is found to be sufficient to obtain the stress intensity factors from the corresponding isotropic results. For mode I and mode II beam specimens, the energy release rates are expressed in such a way that the leading term is the simple beam theory solution. The calibration of mixed

mode beam specimens is much more difficult, since the mode mixity changes with the beam thickness ratio and the crack length.

Attention in this article has been focused on the interplay between material anisotropy and finite geometry. However, material orthotropy may also play an important role in bridging phenomena. In fact, all fracture and fatigue cracking processes in composites are subject to resistances that increase with crack extension, because of various bridging effects. The coupling of material orthotropy and bridging merits further study.

Acknowledgements—Funding of this work was supplied in part by the DARPA University Research Initiative (Subagreement P.O. #VB38639-0 with the University of California, Santa Barbara, ONR Prime contract N-0-0014-86-K-0753). ZS is in addition supported by NSF through a Research Initiation Award MSS-9011571, and by a research grant of the Academic Senate of the University of California. Provision of the ABAQUS finite element code by Hibbitt, Karlsson and Sorensen, Inc. of Providence, RI is gratefully acknowledged.

REFERENCES

Bao, G., Fan, B. and Evans, A. G. (1990). Mixed mode delamination cracking in brittle matrix composites. *Mech. Mater.* (In press).

Boa, G. and McMeeking, R. M. (1991). Fatigue crack growth in fiber-reinforced metal-matrix composite. *J. Mech. Phys. Solids.* (Submitted for publication).

Carlsson, L. A. and Gillespie Jr, J. W. (1989). Mode-II interlaminar fracture of composites. In *Application of Fracture Mechanics to Composite Materials* (Edited by Friedrich), pp. 113–157. Elsevier, New York.

Davies, P. and Benzeggagh, M. L. (1989). Interlaminar mode-I fracture testing. In *Application of Fracture Mechanics to Composite Materials* (Edited by Friedrich), pp. 81–112. Elsevier, New York.

He, M. and Evans, A. G. (1991). Finite element analysis of beam specimens used to measure the delamination resistance of composites. *J. Comp. Tech. Res.* (In press).

Kageyama, K. (1989). Fracture mechanics of notched carbon/epoxy laminates. In *Application of Fracture Mechanics to Composite Materials* (Edited by Friedrich), pp. 327–396. Elsevier, New York.

Lekhnitskii, S. G. (1981). *Theory of Elasticity of an Anisotropic Body*. Mir Publishers, Moscow.

Rice, J. R. (1988). Elastic fracture mechanics concepts for interfacial cracks. *J. Appl. Mech.* **55**, 98–103.

Sih, G. C., Paris, P. C. and Irwin, G. R. (1965). On cracks in rectilinearly anisotropic bodies. *Int. J. Fract. Mech.* **1**, 189–203.

Spearing, S. M. and Evans, A. G. (1991). Delamination fracture of ceramic matrix fiber composites. *Acta Metal. Mater.* (In press).

Suo, Z. (1990a). Delamination specimens for orthotropic materials. *J. Appl. Mech.* **57**, 627–634.

Suo, Z. (1990b). Singularities, interfaces and cracks in dissimilar anisotropic media. *Proc. Roy. Soc. London* **A427**, 331–358.

Suo, Z., Bao, G., Fan, B. and Wang, T. C. (1990). Orthotropy rescaling and implications for fracture in composites. *Int. J. Solids Structures* **28**, 235–248.

Suo, Z., Bao, G. and Fan, B. (1992). Delamination *R*-curve phenomena due to damage. *J. Mech. Phys. Solids.* (In press).

Tada, H., Paris, P. C. and Irwin, G. R. (1985). *The Stress Analysis of Cracks Handbook*. Del Research, St. Louis, MO.

Wang, T. C., Shih, C. F. and Suo, Z. (1990). Crack extension and kinking in laminates and bicrystals. *Int. J. Solids Structures* **29**, 327–344.

APPENDIX

Let the coordinates x, y and z coincide with principal material directions of an orthotropic material. For plane strain problems, the governing equation and the definition of λ and ρ remain unchanged, but the elastic constants need to be replaced by

$$E_1' = E_1/(1-\nu_{13}\nu_{31}), \quad \nu_{12}' = (\nu_{12}+\nu_{13}\nu_{32})/(1-\nu_{13}\nu_{31})$$
$$E_2' = E_2/(1-\nu_{23}\nu_{32}), \quad \nu_{21}' = (\nu_{21}+\nu_{23}\nu_{31})/(1-\nu_{23}\nu_{32}). \tag{A1}$$

There is no need to change the shear modulus, G_{12}. This replacement should be done with all the solutions in the text if the plane strain conditions prevail.